PAPER

Check for updates

Ti$_2$PTe$_2$ monolayer: a promising two-dimensional anode material for sodium-ion batteries†

Jie Liu,[a] Man Qiao,[a] Xiaorong Zhu,[a] Yu Jing [ID] *[bc] and Yafei Li [ID] *[a]

Developing efficient anode materials with a good electrochemical performance has been a key scientific issue in the development of sodium ion batteries (SIBs). In this work, by means of density functional theory (DFT) computations, we demonstrate that two-dimensional (2D) Ti$_2$PTe$_2$ monolayer is a promising candidate for this application. The exfoliation of Ti$_2$PTe$_2$ monolayer from its experimentally known layered bulk phase is feasible due to the moderate cohesive energy. Different from many binary 2D transitions metal chalcogenides (TMCs) that are semiconducting, Ti$_2$PTe$_2$ monolayer is metallic with considerable electronic states at the Fermi level. Remarkably, Ti$_2$PTe$_2$ monolayer has a considerably high theoretical capacity of 280.72 mA h g^{-1}, a rather small Na diffusion barrier of 0.22 eV, and a low average open circuit voltage of 0.31 eV. These results suggest that Ti$_2$PTe$_2$ monolayer can be utilized as a promising anode material for SIBs with high power density and fast charge/discharge rates.

Introduction

In the past few decades, the large-scale exploitation and utilization of fossil fuels has not only led to energy shortages, but also caused serious environmental pollution. Therefore, in recent years, green renewable energy such as solar energy, wind energy and tidal energy has become a hot research topic in scientific community. To this end, the development of related energy storage technologies with high energy density and long cycle life to efficiently store and utilize these renewable energy sources is particularly critical.[1,2] Among current various energy storage technologies, lithium ion batteries (LIBs) have occupied most of the portable electronics market and become the primary choice for energy storage systems, such as electric vehicles and portable mobile device.[3,4] However, the limited lithium (Li) resources on earth would increase the cost of LIBs,[5,6] thereby hindering the large-scale application of LIBs. Sodium (Na) is abundant in nature and low in price, and has similar electrochemical properties to Li. Therefore, secondary batteries based on Na hold the great potential to replace LIBs to become the next generation batteries.[7–11] However, the graphite anode materials that widely used in LIBs cannot be directly applied to sodium ion batteries (SIBs) due to the weak interaction between Na and graphite.[12,13] To this end, developing new anode materials with high specific capacity, high energy density, and good cycle performance is an urgent task for the application of SIBs.

Since the experimental realization of graphene by Geim *et al.* in 2004,[14,15] two-dimensional (2D) materials have gained a lot of interests in the fields of electrochemical energy storage and conversion systems due to its extraordinary properties.[16–18] Especially, both sides of 2D materials can offer ultra-high surface area of for Na adsorption and short distance for Na migration, which make 2D materials rather attractive for SIBs. However, rather few experimentally realized 2D structures can be served as anode materials for SIBs. For example, graphene, which has rather high electronic conductivity, was excluded as the qualified candidate as the adsorption of Na ions on the surface of graphene is energetically unfavorable.[19,20] The single-layered black phosphorus, namely phosphorene,[21,22] was revealed theoretically to have a high Na capacity and a low Na diffusion barrier.[23,24] However, the poor stability of phosphorene in ambient conditions would significantly constraint its application in energy storage.[25] Quite recently, 2D transitions metal chalcogenides (TMCs) were also proposed to be the promising anode materials for SIBs.[26–28] However, many TMCs anodes (*e.g.*, MoS$_2$) suffer from rather inferior capacities and low electronic conductivity. At present, searching for new 2D layered anodes with high Na capacity, low Na diffusion barrier, and high electronic conductivity remains a big challenge.[29–35]

Experimentally, many 2D structures (*e.g.* graphene,[14] MoS$_2$,[36] black phosphorene[22]) have been realized *via* exfoliation strategies from there bulk counterparts, which provides us a feasible

a Jiangsu Key Laboratory of New Power Batteries, Jiangsu Collaborative Innovation Centre of Biomedical Functional Materials, School of Chemistry and Materials Science, Nanjing Normal University, Nanjing 210023, China. E-mail: liyafei@njnu. edu.cn

b College of Chemical Engineering, Nanjing Forestry University, Nanjing 210037, China. E-mail: yujing@njfu.edu.cn

c Jiangsu Co-Innovation Centre of Efficient Processing and Utilization of Forest Resources, Nanjing 210037, China

way to explore new 2D electrodes for SIBs. Recently, several layered ternary TMCs (*e.g.* Ti_2PTe_2,[37–40] Zr_2PTe_2 (ref. 41)) with more than two chalcogens of pnictogen and tellurium with zirconium or titanium cations were synthesized and revealed to be metallic. Inspired by the extensive studies of developing 2D anodes for SIBs, one may naturally wonder whether 2D ternary TMCs could be exfoliated and attractive for SIBs. However, at present the energy storage performance of 2D ternary TMCs remain yet to be explored. Theoretical advances in recent years have made it is possible to evaluate a wide range of essential battery-related properties, such as voltage, ion diffusion, and theoretical capacity.[42–44] Therefore, a theoretical study on this issue will shed some lights on developing novel anodes for SIBs.

In this work, we systematically studied the structural and electronic properties of Ti_2PTe_2 monolayer and explored the possibility of using it as an anode material for SIBs. It is found that Ti_2PTe_2 monolayer is a stable 2D metal and can be easily obtained *via* exfoliation strategies. Remarkably, our results revealed that Ti_2PTe_2 monolayer can provide moderate Na binding strength, low Na diffusion barrier, and higher theoretical capacity than 2D binary TMCs, thus holding great potentials to be utilized as an anode material for SIBs.

Computational details

Our spin-polarized density functional theory (DFT) computations were performed using the plane-wave technique as implemented in Vienna *ab initio* simulation package (VASP).[45] The ion–electron interaction was described using the projector-augmented plane wave (PAW) approach.[46,47] The structural optimization was conducted using the generalized gradient approximation (GGA) expressed by PBE functional[48] while the electronic structure computations were performed by employing the HSE06 hybrid functional method.[49] A 500 eV cutoff energy for the plane-wave basis set was adopted in all computations. The weak interactions were described by adopting the DFT-D3 (D stands for dispersion) method with the Grimme vdW correction.[50] The convergence threshold was set as 10^{-4} eV in energy and 10^{-3} eV $Å^{-1}$ in force. We set the x and y directions parallel and the z direction perpendicular to the layer plane, and adopted a supercell length of 20 Å in the z direction. The 2D Brillouin zone of Ti_2PTe_2 monolayer was sampled with a $4 \times 4 \times 1$ Γ centered k points grid.

The *ab initio* molecular dynamics (AIMD) simulations were carried out to assess the thermal stability of the Ti_2PTe_2 monolayer. The temperature was controlled by using the Nosé–Hoover method.[51] At each temperature, the AIMD simulation with the mount of substance (N), volume (V), and temperature (T) being conserved (NVT ensemble) lasts for 10 ps with a time step of 1.0 fs. The phonon band structure of Ti_2PTe_2 monolayer was computed using the density functional perturbation theory (DFPT)[52] as implemented in the Phonopy program.[53] The climbing-image nudged elastic band (CI-NEB) method[54] as implemented in VASP was employed to simulate the Na diffusion energy barrier on Ti_2PTe_2 monolayer.

Results and discussion

Fig. 1a shows the geometrics of Ti_2PTe_2 bulk, which crystallizes in a hexagonal structure with the space group $R3m$ (no. 166). In Ti_2PTe_2 bulk, Ti_2PTe_2 layers are stacked together with interlayer vdW binding along the z-axis in ABC sequence. The equilibrium lattice parameters of Ti_2PTe_2 bulk were optimized to be $a = 3.66$ Å, $b = 3.66$ Å, and $c = 29.81$ Å at PBE-D3 level of theory, which are in good agreements with the experimentally measured values ($a = 3.64$ Å, $b = 3.64$ Å, $c = 28.49$ Å).[37] The optimized lattice parameters of Ti_2PTe_2 monolayer ($a = 3.64$ Å, $b = 3.64$ Å) are slightly smaller than those of the bulk phase. Each Ti_2PTe_2 monolayer consists of five atomic layers (two Ti layers, one P layer, and two Te layers), which is different to the typical 2D binary TMCs with three atomic layers. In Ti_2PTe_2 monolayer (Fig. 1b), each Ti atom binds with three Te atoms and three P atoms while each P atom solely binds with six Ti atoms. Therefore, the structure of Ti_2PTe_2 can be described as layers of isolated telluride and phosphide anions form an ordered close sphere-packing with titanium cations filling two-thirds of the octahedral voids. The Te–Ti and Ti–P bond lengths are 2.79 and 2.48 Å, respectively. According to the Bader charge population analysis, the Ti, P, and Te atoms in Ti_2PTe_2 monolayer possess a charge of +1.17, −1.36, and −0.49 $|e|$, respectively, which is in accordance with its ionic formula $(Ti^{4+})_2(P^{3-})(Te^{2-})_2(e^{-})$ deduced experimentally.[37]

Since Ti_2PTe_2 monolayer has not been realized experimentally yet, it is necessary for us to access its stability before revealing the properties and potential applications. The stability of Ti_2PTe_2 monolayer can be firstly endorsed by the phonon dispersion curves shown in Fig. 1c, where no imaginary phonon modes can be observed and the highest frequency can
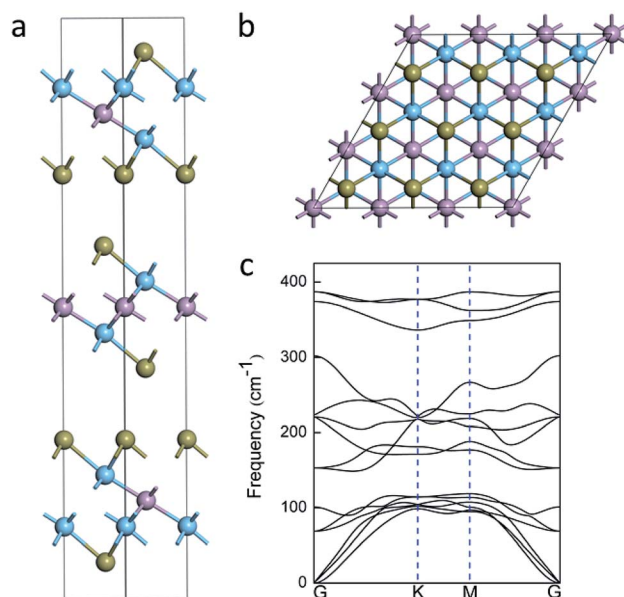

Fig. 1 (a) Side view of the crystal structure of Ti_2PTe_2 bulk. The brown, blue and pink balls represent Te, Ti, and P atoms, respectively. (b) Top view of the optimized structure of Ti_2PTe_2 monolayer. (c) Phonon dispersion curves of Ti_2PTe_2 monolayer.

reach up to 390 cm^{-1}. Therefore, Ti$_2$PTe$_2$ monolayer is a kinetically stable 2D structure. We also carried out the AIMD simulations to assess the thermodynamic stability of Ti$_2$PTe$_2$ monolayer. As shown in Fig. S1,† the geometry of Ti$_2$PTe$_2$ monolayer is not pronouncedly distorted at the temperature of 500 K, suggesting that Ti$_2$PTe$_2$ monolayer has good thermodynamic stability and can work at harsh environments.

The feasibility of producing Ti$_2$PTe$_2$ monolayer *via* the exfoliation strategy was then evaluated by computing the cleavage energy (E_{cl}) of Ti$_2$PTe$_2$, which is defined as the minimum energy required to isolate a monolayer from the bulk. Specifically, the exfoliation process was simulated by imposing a fracture in a five-layer slab model of Ti$_2$PTe$_2$, in which the top layer is removable while the rest four layers are fixed. The distance between two fractures in the equilibrium configuration was defined as zero, and the E_{cl} can be determined *via* increasing the separation distance. As shown in Fig. 2, when the separation distance is larger than 6 Å, the E_{cl} of Ti$_2$PTe$_2$ monolayer gradually converges to a constant value of ∼0.38 J m^{-2}. Remarkably, the E_{cl} of Ti$_2$PTe$_2$ monolayer is quite close to that of graphene (0.37 J m^{-2})[55] and much lower than the experimentally realized Ga$_2$N monolayer (1.09 J m^{-2}),[56] suggesting the high feasibility to extract 2D Ti$_2$PTe$_2$ from its bulk phase in the laboratory.

The good electrical conductivity is essentially required for the excellent electrochemical performance of electrode materials. However, most binary 2D TMCs (*e.g.* MoS$_2$, TiS$_2$) are semiconducting with poor conductivity, which usually requires the addition of conducting materials (*e.g.* graphene) to facilitate the electrochemical reactions. The electronic properties of Ti$_2$PTe$_2$ monolayer were then investigated by computing its electronic band structure and density of states (DOS). As shown in Fig. 3, Ti$_2$PTe$_2$ monolayer is metallic with several energy levels crossing the Fermi level computed at the HSE06 level of theory. According to the partial DOS analysis, the metallic states at the Fermi level are mainly contributed by Ti-3d states.
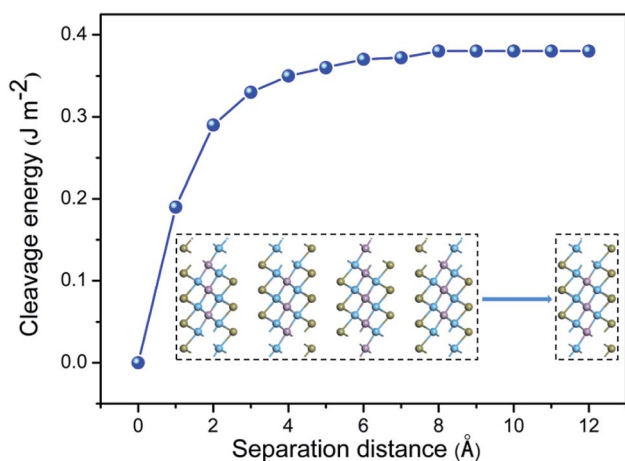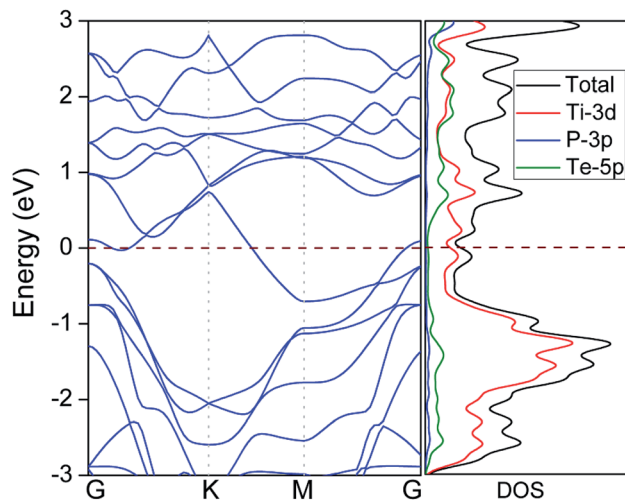

Fig. 3 Band structure (left) and density of states (DOS) (right) of Ti$_2$PTe$_2$ monolayer. The pink dashed lines denote the position of Fermi level.

Therefore, the metallic Ti$_2$PTe$_2$ monolayer stands out to be a highly desirable candidate of anode material for SIBs.

After the thorough understanding on the basic electronic properties of Ti$_2$PTe$_2$ monolayer, it is next accessed whether this novel 2D structure can be served as an anode material for SIBs. To this end, we firstly studied the adsorption of one isolated Na atom on the surface of Ti$_2$PTe$_2$ monolayer by constructing a 3 × 3 supercell. The adsorption energy of Na (E_a) is defined as:

$$E_a = E_{Ti_2PTe_2Na} - E_{Ti_2PTe_2} - \mu_{Na}$$

where $E_{Ti_2PTe_2Na}$ and $E_{Ti_2PTe_2}$ are the total energies of the Na-adsorbed Ti$_2$PTe$_2$ monolayer and bare Ti$_2$PTe$_2$ monolayer, respectively. μ_{Na} is the chemical potential of Na and is taken as the cohesive energy of bulk Na. According to our definition, a negative value of adsorption energy means that the Na atom prefers to be adsorbed on the monolayer instead of forming a bulk metal, and a more negative adsorption energy indicates the more favorable interaction between Ti$_2$PTe$_2$ monolayer and Na.

Considering the symmetry of Ti$_2$PTe$_2$ monolayer, three possible Na adsorption sites can be identified (Fig. 4), including the hollow site (H) above the center of a Ti$_3$Te$_3$ hexagon, the top site above one Ti atom (T$_1$), and the top site directly above one Te atom (T$_2$). Actually, the Na adsorption on H and T$_1$ sites are expected to have interactions with three surrounding Te atoms. The adsorption energies of all these three sites were computed to determine the most favorable adsorption configuration for Na. According to our computations, the three considered sites all have a negative adsorption energy, indicating that the Na storage on Ti$_2$PTe$_2$ monolayer could be exothermic and spontaneous. In particular, the T$_1$ site has the most negative adsorption energy (−1.17 eV), followed by H site (−1.14 eV) and T$_2$ site (−0.56 eV). The distance between the adsorbed Na atom and the neighboring Te atoms were optimized to be 2.69, 2.64, and 2.86 Å for T$_1$, H, and T$_2$, respectively. Remarkably, the Na
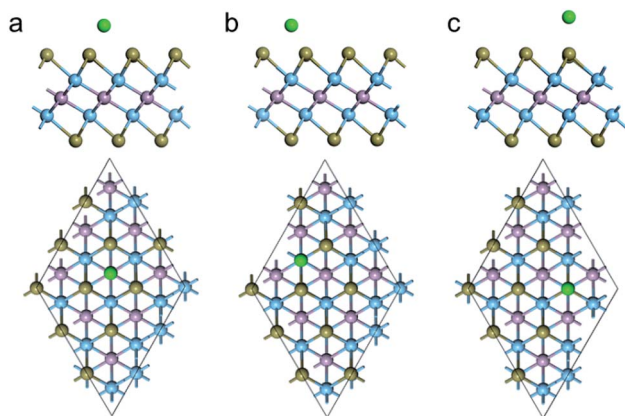

Fig. 2 Cleavage energy as a function of the separation distance for a fracture in bulk Ti$_2$PTe$_2$. Inset is the schematic of separating a Ti$_2$PTe$_2$ monolayer from its neighboring four-layer.

Fig. 4 Side (upper) and top (bottom) views of the optimized structures for Na adsorption on the (a) H, (b) T_1, and (c) T_2 sites of Ti_2PTe_2 monolayer. The green ball represents Na atom.

Fig. 5 (a) Migration paths and (b) diffusion barrier profile for Na on the surface of Ti_2PTe_2 monolayer.

adsorption on Ti_2PTe_2 monolayer has not lead to appreciable geometric change or lattice expansion, indicative of great stability that is favorable for SIBs applications. According to the Bader charge population analysis, the adsorbed Na atom possesses a positive charge of 0.76, 0.75, and 0.81$|e|$ at T_1, H, and T_2 site, respectively, indicating that the adsorbed Na are pronouncedly ionized and the interaction between Ti_2PTe_2 monolayer and Na is mainly of the Coulomb interaction.

The density of states (DOS) of Ti_2PTe_2 monolayer with the adsorbed Na at three different sites were then examined. As clearly shown in Fig. S2,† the adsorption of Na does not significantly change the overall electronic properties of Ti_2PTe_2 monolayer except for the upshift of Fermi level. Therefore, Ti_2PTe_2 monolayer can maintain its metallic nature after the adsorption of Na, which is an advantage for its applications as battery electrodes.

We then turned our attention to the motion of Na on the surface of Ti_2PTe_2 monolayer as the rate performance of a battery electrode is mainly determined by the mobility of intercalated metal ions. Here the motion of Na on Ti_2PTe_2 monolayer was evaluated by using the CI-NEB method to determine the minimum-energy pathways and estimate the diffusion barriers. The adsorption configuration of Na atom on Ti_2PTe_2 monolayer (T_1 site) was used as the initial state while the configuration with Na adsorption at a neighboring T_1 site was chosen to be the final state. As shown in Fig. 5, two possible migration pathways, which correspond to the diffusion of Na between two neighboring T_1 sites passing through a P atom (viewed from top) (path 1) or passing through a Te atom (path 2) were identified. According to our CI-NEB computations, the diffusion barrier of path 1 (0.22 eV) is much lower than that of path 2 (0.67 eV). These results are in good agreements with our computations of the adsorption energy. Encouragingly, the obtained Na diffusion barriers on the surface of Ti_2PTe_2 monolayer are actually rather low and comparable to those of MoS_2,[28] phosphorene,[24] and graphene materials.[57] Therefore, Na can diffuse rather fast on the surface of Ti_2PTe_2 monolayer,
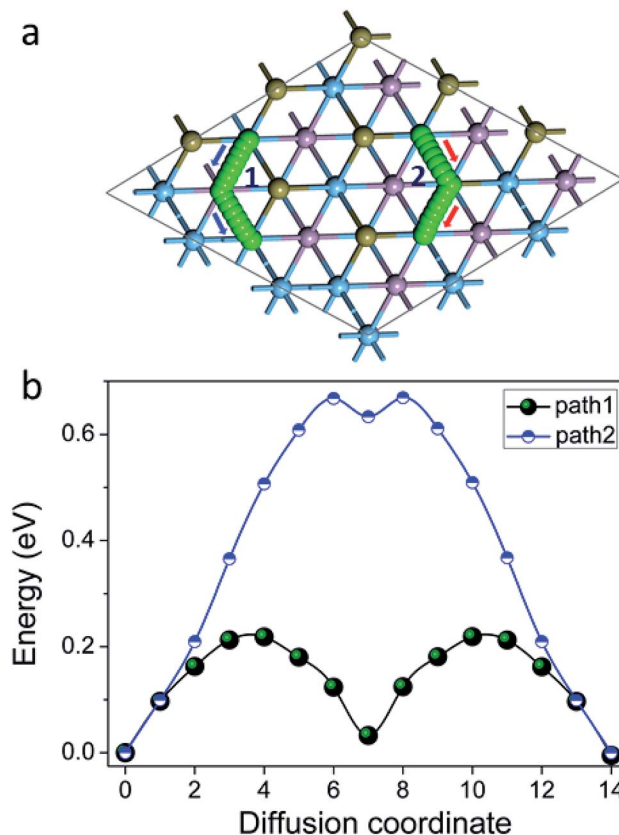
and good rate capability can be expected for Ti_2PTe_2 monolayer when it is utilized as the anode material in SIBs.

For practical application, the Na storage capacity is the key indicator for the performance of electrode materials for SIBs. Therefore, we further estimated the theoretical Na storage capacity for Ti_2PTe_2 monolayer, which is defined as the maximum capacity that still shows a negative average adsorption energy. Here we employed a $3 \times 3 \times 1$ supercell as the model for extra Na storage. Considering that previous studies have demonstrated that the multilayer Na adsorption can significantly enhance the capacities of 2D anodes,[30,31] we also allowed that the concentration of adsorbed Na on Ti_2PTe_2 monolayer increasing layer by layer on both sides simultaneously. Specifically, the first layer of Na atoms are adsorbed on the T_1 sties, which are the most stable sites for Na adsorption. After the T_1 sites are occupied completely, the Na atoms will be adsorbed at H sites to form the second layer. Similarly, Na atoms in the third layer would be adsorbed on the top of Se atoms. To evaluate the interaction between Na atoms and the host material, we computed the average adsorption energies of Na atoms in each layer (E_{ave}), which is defined as:

$$E_{ave} = \frac{E_{Ti_2PTe_2-Na_{18n}} - E_{Ti_2PTe_2-Na_{18(n-1)}} - 18\mu_{Na}}{18}$$

where $E_{Ti_2PTe_2-Na_{18n}}$ and $E_{Ti_2PTe_2-Na_{18(n-1)}}$ are the total energies of Ti_2PTe_2 monolayer with n and $(n-1)$ layers of adsorbed Na. The

number "18" in the formula means that eighteen Na atoms are adsorbed in each layer (for a $3 \times 3 \times 1$ supercell and on both sides).

According to our computations, the average adsorption energy of first Na layer is -0.49 eV, implying the strong interaction between these Na ions and Ti_2PTe_2 monolayer. In contrast, the average adsorption energy of the second Na layer rapidly decreases to -0.13 eV. Nevertheless, the negative average adsorption energy can still ensure good intercalation stability of these Na ions on Ti_2PTe_2 monolayer. However, the average adsorption energy of the third Na layer becomes positive, indicating that the adsorption of these Na ions is energetically unfavorable and they would tend to form undesirable Na dendrites. Therefore, our computations reveals that the maximum number of Na storage for a $3 \times 3 \times 1$ supercell of Ti_2PTe_2 monolayer is 36, corresponding to the chemical stoichiometry of $Na_4Ti_2PTe_2$ (Fig. 6). As a result, the theoretical specific capacity of Ti_2PTe_2 monolayer as anode of SIBs is ~ 280.72 mA h g^{-1}, which is much higher than those of MoS_2 monolayer and Mxene. Especially, during the intercalation of Na ions on Ti_2PTe_2 monolayer, the lattice constants in the x–y plane of intercalated compounds only increase slightly ($\sim 1\%$). This very small strain is another great advantage of Ti_2PTe_2 monolayer to be used as an electrode for rechargeable batteries. Moreover, it is found that the metallic feature of Ti_2PTe_2 monolayer can be well kept after adding two Na layers in both sides (Fig. S3†).

Experimentally, the voltage has been well employed as a discriminator in screening the suitable anode materials for SIBs, and it is accepted that a voltage in the range of 0.0–1.0 V is suitable to maximize the energy density as well as avoid the formation of Na dendrites. To this end, we also computed the average open circuit voltage (OCV) for Na intercalation on Ti_2PTe_2 monolayer. Typically, the anode charge/discharge processes assume the following half–cell reaction vs. Na/Na^+
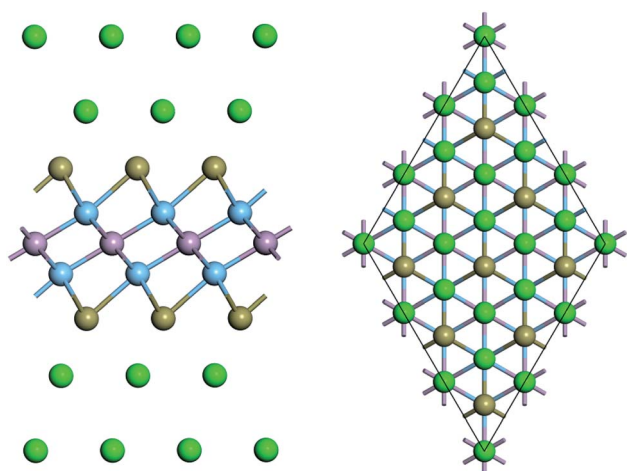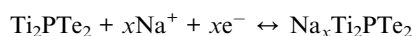
$$Ti_2PTe_2 + xNa^+ + xe^- \leftrightarrow Na_xTi_2PTe_2$$

With the effects of volume and entropy being both neglected, the OCV for Na intercalation on Ti_2PTe_2 monolayer can be computed from the total energy difference on the basis of following equation by neglecting the:[58]

$$OCV \approx \frac{E_{Na_{x_2}Ti_2PTe_2} - E_{Na_{x_1}Ti_2PTe_2} + (x_2 - x_1)\mu_{Na}}{(x_2 - x_1)e}$$

where $E_{Na_{x_2}Ti_2PTe_2}$ and $E_{Na_{x_1}Ti_2PTe_2}$ are the total energies of Ti_2PTe_2 monolayer with Na concentrations limits of x_2 and x_1, respectively. According to our computations, when Ti_2PTe_2 monolayer reaches the highest Na capacity, corresponding to the case of $x_1 = 0$ and $x_2 = 4$, the average OCV is 0.31 V, which is lower than those of most 2D binary TMCs.[28] Therefore, Ti_2PTe_2 monolayer should be a rather good candidate of electrode material for SIBs.

Conclusion

To summarize, by means of comprehensive DFT computations, we systematically studied the structural, electronic, and energy storage properties of Ti_2PTe_2 monolayer. According to our computational results, Ti_2PTe_2 monolayer is a stable 2D structure and could be realized experimentally via exfoliation strategies. Remarkably, Ti_2PTe_2 monolayer has a rather small Na diffusion barrier and it can stably accommodate Na up to Na_4-Ti_2PTe_2 with an open circuit voltage of 0.31 V. Especially, Ti_2PTe_2 monolayer is metallic with excellent electronic conductivity. With all of these extraordinary properties, Ti_2PTe_2 monolayer would have a great potential to be utilized as an anode material for SIBs. Due to the high experimental feasibility, it is expected that Ti_2PTe_2 monolayer could be realized in the lab in the quite near future. We also hope our studies could stimulate more theoretical and experimental efforts on developing 2D ternary TMCs for energy storage applications.

Conflicts of interest

There are no conflicts to declare.

Acknowledgements

Fig. 6 Side (left) and top (right) views of optimized geometric structure of $Na_4Ti_2PTe_2$.

References

1 H. Chen, T. N. Cong, W. Yang, C. Tan, Y. Li and Y. Ding, *Prog. Nat. Sci.*, 2009, **19**, 291.

2 B. Dunn, H. Kamath and J.-M. Tarascon, *Science*, 2011, **334**, 928.

3 J. M. Tarascon and M. Armand, *Nature*, 2001, **414**, 359.

4 D. P. Dubal, O. Ayyad, V. Ruiz and P. Gomez-Romero, *Chem. Soc. Rev.*, 2015, **44**, 1777.

5 https://en.wikipedia.org/wiki/File:Elemental_abundances.svg.

6 J. B. Goodenough and K.-S. Park, *J. Am. Chem. Soc.*, 2013, **135**, 1167.

7 N. Yabuuchi, K. Kubota, M. Dahbi and S. Komaba, *Chem. Rev.*, 2014, **114**, 11636.

8 M. D. Slater, D. Kim, E. Lee and C. S. Johnson, *Adv. Funct. Mater.*, 2013, **23**, 947.

9 H. Pan, Y. –S. Hu and L. Chen, *Energy Environ. Sci.*, 2013, **6**, 2338.

10 W. Luo, F. Shen, C. Bommier, H. Zhu, X. Ji and L. Hu, *Acc. Chem. Res.*, 2016, **49**, 231.

11 J. –Y. Hwang, S. –T. Myung and Y. –K. Sun, *Chem. Soc. Rev.*, 2017, **46**, 3529.

12 S. P. Ong, V. L. Chevrier, G. Hautier, A. Jain, C. Moore, S. Kim, X. Ma and C. Ceder, *Energy Environ. Sci.*, 2011, **4**, 3680.

13 S. Y. Hong, Y. Kim, Y. Park, A. Choi, N. –S. Choi and K. T. Lee, *Energy Environ. Sci.*, 2013, **6**, 2067.

14 K. S. Novoselov, A. K. Geim, S. V. Morozov, D. Jiang, Y. Zhang, S. V. Dubonos, I. V. Gregorieva and A. A. Firsov, *Science*, 2004, **306**, 666.

15 K. S. Novoselov, D. Jiang, F. Schedin, T. J. Booth, V. V. Khotkevich, S. V. Morozov and A. K. Geim, *Proc. Natl. Acad. Sci. U. S. A.*, 2005, **102**, 10451.

16 K. S. Novoselov, V. I. Falko, L. Colombo, P. R. Gellert, M. G. Schwab and P. Kim, *Nature*, 2012, **490**, 192.

17 R. Raccichini, A. Varzi, S. Passerini and B. Scrosati, *Nat. Mater.*, 2015, **14**, 271.

18 C. Xu, B. Xu, Y. Gu, Z. Xiong, J. Sun and X. S. Zhao, *Energy Environ. Sci.*, 2013, **6**, 2067.

19 Y. Liu, B. Merinov and W. A. Goddard, *Proc. Natl. Acad. Sci. U. S. A.*, 2016, **113**, 3735.

20 M. S. Balogun, Y. Luo, W. Qiu, P. Liu and Y. Tong, *Carbon*, 2016, **98**, 162.

21 H. Liu, A. T. Neal, Z. Zhu, D. Tomanek and P. D. Ye, *ACS Nano*, 2014, **8**, 4033.

22 L. Li, Y. Yu, G. J. Ye, Q. Ge, X. Ou, H. Wu, D. Feng, X. H. Chen and Y. Zhang, *Nat. Nanotechnol.*, 2014, **9**, 372.

23 J. Sun, H. –W. Lee, M. Pasta, H. Yuan, G. Zheng, Y. Sun, Y. Li and Y. Cui, *Nat. Nanotechnol.*, 2017, **10**, 980.

24 V. V. Kulish, O. I. Malyi, C. Persson and P. Wu, *Phys. Chem. Chem. Phys.*, 2015, **17**, 13921.

25 J. O. Island, G. A. Steele, H. S. J. Van Der Zant and A. Castellanos-gomez, *2D Mater.*, 2015, **2**, 011002.

26 L. David, R. Bhandavat and G. Singh, *ACS Nano*, 2014, **8**, 1759–1770.

27 J. Zhou, L. Wang, M. Yang, J. Wu, F. Chen, W. Huang, N. Han, H. Ye, F. Zhao, Y. Li and Y. Li, *Adv. Mater.*, 2017, **29**, 1702061.

28 E. Yang, H. Ji and Y. Jung, *J. Phys. Chem. C*, 2015, **119**, 26374.

29 T. Yu, Z. Zhao, L. Liu, S. Zhang, H. Xu and G. Yang, *J. Am. Chem. Soc.*, 2018, **140**, 5962.

30 J. Hu, B. Xu, S. A. Yang, S. Guan, C. Ouyang and Y. Yao, *ACS Appl. Mater. Interfaces*, 2015, **7**, 24016.

31 X. Zhang, Z. Yu, S. –S. Wang, S. Guan, H. Y. Yang, Y. Yao and S. A. Yang, *J. Mater. Chem. A*, 2016, **4**, 15224.

32 G. Chen, Y. Bai, H. Li, Y. Li, Z. Wang, Q. Ni, L. Liu, F. Wu, Y. Yao and C. Wu, *ACS Appl. Mater. Interfaces*, 2017, **9**, 6666.

33 X. Zhang, J. Hu, Y. Cheng, H. Y. Yang, Y. Yao and S. A. Yang, *Nanoscale*, 2016, **8**, 15340.

34 X. Zhang, Z. Zhang, S. Yao, A. Chen, X. Zhao and Z. Zhou, *npj Comput. Mater.*, 2018, **4**, 13.

35 C. –S. Liu, X. –L. Yang, J. Liu and X. –J. Ye, *ACS Appl. Energy Mater.*, 2018, **1**, 3850.

36 K. F. Mak, C. Lee, J. Hone, J. Shan and T. F. Heinz, *Phys. Rev. Lett.*, 2010, **105**, 136805.

37 F. Philipp, P. Schmidt, M. Ruck, W. Schnelle and A. Isaeva, *J. Solid State Chem.*, 2008, **181**, 2859.

38 F. Philipp, P. Schmidt, E. Milke, M. Binnewies and S. Hoffmann, *J. Solid State Chem.*, 2008, **181**, 758.

39 T. Yajima, M. Koshiko, Y. Zhang, T. Oguchi, W. Yu, D. Kato, Y. Kobayashi, Y. Orikasa, T. Yamamoto, Y. Uchimoto, M. A. Green and H. Kageyama, *Nat. Commun.*, 2016, **7**, 13809.

40 J. S. Oh, H. –S. Yu, C. –J. Kang, S. Sinn, M. Han, Y. J. Chang, B. –G. Park, K. Lee, B. I. Min, S. W. Kim, H. –D. Kim and T. W. Noh, *Chem. Mater.*, 2016, **28**, 7570.

41 K. Tschulik, M. Ruch, M. Binnewies, E. Milke, S. Hoffmann, W. Schnelle, B. P. T. Fokwa, M. Gillesen and P. Schmidt, *Eur. J. Inorg. Chem.*, 2009, **21**, 3102.

42 Z. Deng, Y. Mo and S. P. Ong, *NPG Asia Mater.*, 2016, **8**, e254.

43 Y. Wang, W. D. Richards, S. P. Ong, L. J. Miara, J. C. Kim, Y. Mo and G. Ceder, *Nat. Mater.*, 2015, **14**, 1026.

44 Q. Bai, L. Yang, H. Chen and Y. Mo, *Adv. Energy Mater.*, 2018, **8**, 1702998.

45 G. Kresse and J. Hafner, *Phys. Rev. B: Condens. Matter Mater. Phys.*, 1993, **47**, 558.

46 P. E. Blöchl, *Phys. Rev. B: Condens. Matter Mater. Phys.*, 1994, **50**, 17953.

47 G. Kresse and D. Joubert, *Phys. Rev. B: Condens. Matter Mater. Phys.*, 1999, **59**, 1758.

48 J. P. Perdew, L. Burke and M. Ernzerhof, *Phys. Rev. Lett.*, 1996, **77**, 3865.

49 J. Heyd, G. E. Scuseria and M. Ernzerhof, *J. Chem. Phys.*, 2006, **124**, 219906.

50 S. Grimme, *J. Comput. Chem.*, 2007, **27**, 1787.

51 G. J. Martyna, M. L. Klein and M. E. Tuckerman, *J. Chem. Phys.*, 1992, **97**, 2635.

52 S. Baroni, S. De Gironcoli, A. Dal Corso and P. Giannozzi, *Rev. Mod. Phys.*, 2001, **73**, 515.

53 A. Togo, F. Oba and I. Tanaka, *Phys. Rev. B: Condens. Matter Mater. Phys.*, 2008, **78**, 134106.

54 G. Henkelman, B. P. Uberuaga and H. Jonsson, *J. Chem. Phys.*, 2000, **113**, 9901.

55 R. Zacharia, H. Ulbricht and T. Hertel, *Phys. Rev. B: Condens. Matter Mater. Phys.*, 2004, **69**, 155406.

56 S. Zhao, Z. Li and J. Yang, *J. Am. Chem. Soc.*, 2014, **136**, 13313.

57 C. Ling and F. Mizuno, *Phys. Chem. Chem. Phys.*, 2014, **16**, 10419.

58 M. K. Aydinol, A. F. Kohan, G. Ceder, K. Cho and J. Joannopoulos, *Phys. Rev. B: Condens. Matter Mater. Phys.*, 1997, **56**, 1354.